A Uniformly Semiglobally Exponentially Stable Nonlinear Observer for GNSS- and Camera-Aided Inertial Navigation

L. Fusini, T. I. Fossen and T. A. Johansen

***Abstract*— In this paper a nonlinear observer design for estimation of position, velocity, acceleration, attitude and gyro bias of an Unmanned Aerial Vehicle (UAV) is proposed. The sensor suite consists of an Inertial Measurement Unit (IMU), a Global Navigation Satellite System (GNSS) receiver, a video camera and an altimeter. The camera and machine vision can track features from the environment and calculate the optical flow. These data, together with those from the other sensors, are fed to the observer, that is proven to be uniformly semiglobally exponentially stable (USGES). The performance of the observer is tested on simulated data by assuming that the camera system can provide the necessary information.**

I. Introduction

Navigation can be defined as "the task of determining an object's position, velocity, or attitude by combining information from different sources" [1]. A good estimator for such values is the extended Kalman filter, but its computational footprint makes it a demanding solution for systems with low computational power, for example small unmanned vehicles. Researchers have then started developing nonlinear observers as alternatives to the Kalman filter, producing several and diverse results with stability proofs and experimental support. The problem of attitude estimation has received significant attention as a stand-alone problem [2], [3], [4], [5], [6], [7], [8]. As a step forward, other researchers have considered the integration of Inertial Navigation System (INS), magnetometer/compass and GNSS to estimate attitude, position and velocity of a vehicle.

[9] expanded the vector-based observer proposed by [5] and [6] to include GNSS velocity measurements. [2] and [3] built globally exponentially stable (GES) attitude estimators based on multiple time-varying reference vectors or a single persistently exiting vector. A similar observer was developed in [1] to include also gyro bias and GNSS integration. An extension of this [10] replaced the rotation matrix with the unit quaternion for representing attitude, considered Earth rotation and curvature, a non-constant gravity vector, and included accelerometer bias estimation.

Besides GNSS and IMU, another sensor commonly used in navigation is the camera: its greatest advantages are low weight, low power consumption and the availability of a wide range of machine vision software tools that make it an extremely versatile device. Drawbacks are its dependence on lighting and weather conditions, on the existence of suitable image features for image processing, and the difficulty in separating camera motion from moving objects in complex non-stationary environments.

[11] and [12] derived an implicit extended Kalman filter (EKF) that could recover the camera motion states. Such work has been later extended [13] to include aircraft dynamics into the implicit EKF. In [14] a single camera is used to reduce the drift over time of an IMU unassisted by GNSS.

Optical flow (OF) from a single camera is used in [15] to estimate body axes angular rates of an aircraft as well as wind-axes angles in a GPS-denied scenario. A single camera and the OF obtained through it is also exploited for obstacle avoidance in [16]. A comparative study on the accuracy of different OF algorithms is presented in [17].

A. Contribution of this Paper

This paper proposes a nonlinear observer for position, velocity, acceleration, attitude and gyro bias of a UAV. It is shown that the equilibrium point of the estimation error dynamics is USGES. Exponential stability is important for systems that are exposed to environmental disturbances and uncertain initialisation, since it guarantees strong convergence and robustness properties. This, together with having a small computational footprint, constitutes an advantage over other popular algorithms as the EKF.

The system is also fault-tolerant, since the camera may be used to replace the magnetometers in the not unlikely event they present a faulty behaviour.

II. Notation and Preliminaries

Vectors and matrices are represented by lowercase and uppercase letters respectively. X^{-1}, X^{+}, and $\mathrm{tr}(X)$ denote the inverse, pseudoinverse, and trace of a matrix respectively, X^T the transpose of a matrix or vector. The estimated value of X is represented as $\hat{X}$ and the estimation error is defined as $\tilde{X} = X - \hat{X}$. The operator $\|\cdot\|$ denotes the Euclidean norm, I_n the identity matrix of order n and $0_{m\times n}$ the $m \times n$ matrix of zeros. A vector $x = [x_1, x_2, x_3]^T$ is represented in homogeneous coordinates as $\underline{x} = [x_1, x_2, x_3, 1]^T$. The function $\mathrm{sat}(\cdot)$ performs a component-wise saturation of its vector or matrix argument to the interval $[-1, 1]$. The operator $S(x)$ transforms the vector x into the skew-symmetric matrix

$$S(x) = \begin{bmatrix} 0 & -x_3 & x_2 \\ x_3 & 0 & -x_1 \\ -x_2 & x_1 & 0 \end{bmatrix}$$

The inverse operation is denoted as $\mathrm{vex}(\cdot)$, such that $\mathrm{vex}(S(x)) = x$. For a square matrix A, its skew-symmetric part is represented by $\mathbb{P}_a(A) = \frac{1}{2}(A - A^T)$.

L. Fusini, T. I. Fossen and T. A. Johansen are with the Centre for Autonomous Marine Operations and Systems, Dept. of Engineering Cybernetics at NTNU, NO-7491 Trondheim, Norway. E-mail: {lorenzo.fusini, thor.fossen, tor.arne.johansen}@itk.ntnu.no

The frames of reference considered in the paper are the body-fixed frame $\{\mathrm{B}\}$, the North-East-Down (NED) frame $\{\mathrm{N}\}$ (Earth-fixed, considered inertial) and the camera frame $\{\mathrm{C}\}$. The rotation from frame $\{\mathrm{B}\}$ to $\{\mathrm{N}\}$ is represented by matrix $R_b^n \equiv R \in SO(3)$, where $SO(3)$ represents the Special Orthogonal group. The camera is assumed to be fixed to the body and perfectly aligned to it, so that camera-frame and body-frame represent the same coordinate system and can be identified by $\{\mathrm{B}\}$ alone.

A vector decomposed in $\{\mathrm{B}\}$ and $\{\mathrm{N}\}$ has superscript ^{b} and ^{n} respectively. The body (camera) location w.r.t. $\{\mathrm{N}\}$ is identified by $c^n = [c_x^n, c_y^n, c_z^n]^T$. A point in the environment expressed w.r.t. $\{\mathrm{N}\}$ is $t^n = [x^n, y^n, z^n]^T$: note that a point located on the sea surface has $z^n = 0$ and such it will be throughout the paper. The same point expressed w.r.t. $\{\mathrm{B}\}$ is $t^b = [x^b, y^b, z^b]^T$. It will also be assumed that every point is fixed w.r.t. $\{\mathrm{N}\}$. The greek letters ϕ, θ, and ψ represent the roll, pitch, and yaw angles respectively, defined according to the zyx convention for principal rotations. A 2-D camera image has coordinates $[r, s]^T$, aligned with the y^b- and z^b-axis respectively (see Fig. 1). The derivative $[\dot{r}, \dot{s}]^T$ of the image coordinates is the optical flow (OF). Subscript $_F$ indicates a quantity evaluated by means of the OF.

A. Measurements

The sensor suite consists of a GNSS receiver, an IMU, a camera, an altimeter and an inclinometer, providing the following information:

- *GNSS receiver*: NED position p^n and velocity v^n;
- *IMU*: biased angular velocity $\omega_m^b = \omega^b + b$, where b represent the bias, and acceleration a^b;
- *camera*: 2-D projections $[r, s]^T$ onto the image plane of points $[x^n, y^n, z^n]^T$ from the 3-D world;
- *altimeter*: altitude c_z^n;
- *inclinometer*: roll ϕ and pitch θ angles.

A magnetometer, providing the magnetic field m^b, can also be used for redundancy in the observer.

III. Optic Flow Equations

Matrix R and vector c^n represent a rotation and a translation and can be joined to form a 4x4 transformation matrix T from $\{\mathrm{B}\}$ to $\{\mathrm{N}\}$ with homogeneous coordinates

$$T = \begin{bmatrix} R & c^n \\ 0_{1\mathrm{x}3} & 1 \end{bmatrix}$$

such that $\underline{t}^n = T(\phi, \theta, \psi)\ \underline{t}^b$. The inverse transformation is then represented as

$$\underline{t}^b = T^{-1}\underline{t}^n = \begin{bmatrix} R^T & -R^T c^n \\ 0_{1\mathrm{x}3} & 1 \end{bmatrix} \underline{t}^n \tag{1}$$

and $\underline{t}^b$ is a function of $x^n, y^n, c_x^n, c_y^n, c_z^n, \phi, \theta$, and ψ.

The relationship between t^b and its projection onto the image plane is expressed by means of the well-known *pinhole camera model* [18]:

$$\begin{bmatrix} r \\ s \end{bmatrix} = \frac{f}{x^b} \begin{bmatrix} y^b \\ z^b \end{bmatrix}, \quad x^b \neq 0 \tag{2}$$

where f is the focal length, defined as the distance between the image centre o^{rs} and the camera aperture o^b, as in Fig. 1. Note that x^b would be 0 only if the camera had a field

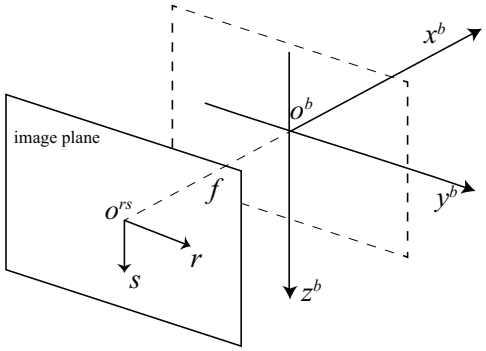

Fig. 1. Pinhole camera model

of view of 180°, a situation that is not contemplated in the present paper. x^b, y^b, z^b in (2) can be replaced by the expressions found through (1), then (2) can be inverted to express x^n and y^n, renamed x_T^n and y_T^n, as functions of $f, r, s, c_x^n, c_y^n, c_z^n, \phi, \theta$, and ψ.

Such x_T^n, y_T^n can then be used as a new t_T^n and transformed again through T^{-1} to give the same point in body coordinates, $\underline{t}_T^b = T^{-1}\underline{t}_T^n$. The resulting t_T^b is then a function of f, r, s, ϕ, θ, and c_z^n.

At this point the OF is considered. For every single point t_T^b tracked by the camera, the relationship between OF and linear/angular velocity in $\{\mathrm{B}\}$ is given by

$$\begin{bmatrix} \dot{r} \\ \dot{s} \end{bmatrix} = M(f, r, s, \phi, \theta, c_z^n) \begin{bmatrix} v_F^b \\ \omega_F^b \end{bmatrix} \tag{3}$$

M is a 2×6 matrix defined in [17]. Assuming that the centre of rotation and the centre of $\{\mathrm{B}\}$ coincide, then M has the structure

$$M = \frac{f}{x_T^b} \begin{bmatrix} -\frac{y_T^b}{x_T^b} & 1 & 0 & -z_T^b & -\frac{y_T^b z_T^b}{x_T^b} & \frac{{y_T^b}^2}{x_T^b} + x_T^b \\ -\frac{z_T^b}{x_T^b} & 0 & 1 & -y_T^b & -\frac{{z_T^b}^2}{x_T^b} - x_T^b & \frac{y_T^b z_T^b}{x_T^b} \end{bmatrix} \tag{4}$$

If the points being tracked were k, then the OF vector would have dimension $2k$ and $M \in \mathbb{R}^{2k \times 6}$: every new tracked point adds two rows to the OF vector and two rows to M, with a structure given by (4). The parameters f, r and s are known from the camera, ϕ, θ are estimated by the attitude observer (see Section IV), c_z^n is measured by the altimeter, so the whole matrix is known. Pseudoinversion allows to express body-fixed velocities as function of OF and t_T^b.

$$\begin{bmatrix} v_F^b \\ \omega_F^b \end{bmatrix} = (M^T M)^{-1} M^T \begin{bmatrix} \dot{r}_1 \\ \dot{s}_1 \\ \vdots \\ \dot{r}_k \\ \dot{s}_k \end{bmatrix} \tag{5}$$

The pseudoinverse of M can be computed as in (5) if $M^T M$ has full rank for all states, which can happen only if $k \geq 3$. The number of features extracted by a chosen image processing algorithm depends on the kind of images available, which in turn depends on the kind of environment

being overflown, lighting and weather conditions, etc. It is assumed that algorithms and flight conditions are good enough to consider $k \geq 3$ and allow Assumption 1 (see Section IV-A).

IV. Observer Design

A. Assumptions

In designing the nonlinear observer the following assumptions are made:

Assumption 1: a sufficient number of image features are selected such that M has full rank and Eq. (5) can be used.

Assumption 2: the gyro bias b is constant, and there exists a known constant $L_b > 0$ such that $\|b\| \leq L_b$.

Assumption 3: there exists a constant $c_{obs} > 0$ such that, $\forall t \geq 0,\ \|v_F^b \times a^b\| \geq c_{obs}$.

Assumption 3 imposes that vectors v_F^b and a^b are non-collinear, i.e. the angle between them is non-zero and none of them can be identically zero (see, e.g., [9], [5]). In practise this condition restricts the types of manoeuvres that insure a correct functioning of the proposed observer. Velocity and accelerations are not an issue for fixed-wing UAVs, since they always have a positive forward speed during flight and never accelerate just opposite to gravity, but helicopter-like vehicles will violate Assumption 3 when in hover or when just gaining altitude and the observer will not work.

The following simplifying assumption is also introduced:

Assumption 4: Euler angles are considered as measured by inclinometers and not extracted from the estimated $\hat{R}$ matrix (i.e. $\hat{R}$ is not fed back to M) as well as the altitude c_z^n, so that matrix M and subsequently v_F^b depend only on known values.

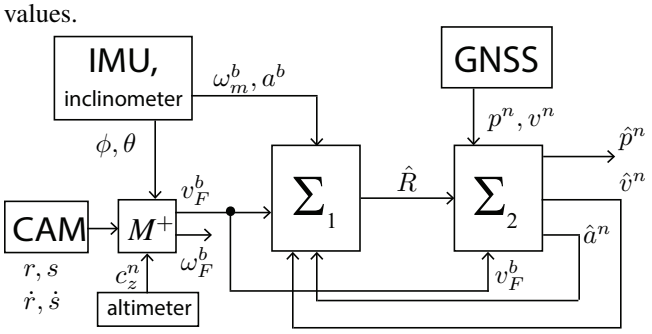

Fig. 2. The actual system being analysed, with Σ_1 representing the attitude observer and Σ_2 the translational motion observer. $\hat{R}$ is not fed back to the camera block, Euler angles are considered as measured by the IMU.

B. Observer Equations

The observer is chosen as

$$\Sigma_1 \begin{cases} \dot{\hat{R}} = \hat{R}S(\omega_m^b - \hat{b}) + \sigma K_P \hat{J} \\ \dot{\hat{b}} = \text{Proj}(\hat{b}, -k_I \text{vex}(\mathbb{P}_a(\hat{R}_s^T K_P \hat{J}))) \end{cases} \tag{6}$$

$$\Sigma_2 \begin{cases} \dot{\hat{p}}^n = \hat{v}^n + K_{pp}(p^n - \hat{p}^n) + K_{pv}(v^n - \hat{v}^n) \\ \dot{\hat{v}}^n = \hat{a}^n + g^n + K_{vp}(p^n - \hat{p}^n) + K_{vv}(v^n - \hat{v}^n) \\ \dot{\xi} = -\sigma K_P \hat{J} a^b + K_{\xi p}(p^n - \hat{p}^n) + K_{\xi v}(v^n - \hat{v}^n) \\ \hat{a}^n = \hat{R}a^b + \xi \end{cases} \tag{7}$$

$$\text{OF}\left\{ \begin{bmatrix} \hat{v}_F^b \\ \hat{\omega}_F^b \end{bmatrix} = \hat{M}^+ \begin{bmatrix} \dot{r} \\ \dot{s} \end{bmatrix} \right. \tag{8}$$

(6)–(7) are the same as in [1], with the only difference being how the matrix J is defined. In addition there is Eq. (8), given by machine vision. The subsystem Σ_1 represents the attitude observer, in which K_P is a symmetric positive definite gain matrix, $\sigma \geq 1$ is a scaling factor tuned to achieve stability, k_I is a positive scalar gain, $\text{Proj}(\cdot,\cdot)$ represents a parameter projection [19] that ensures that $\|\hat{b}\|$ does not exceed a design constant $L_{\hat{b}} > L_b$ (see Appendix). The matrix $\hat{J}$ is the output injection term, whose design is inspired by the TRIAD algorithm [20]. It is defined as

$$\hat{J}(v_F^b,\, \hat{v}^n, a^b, \hat{a}^n, \hat{R}) := \hat{A}_n A_b^T - \hat{R} A_b A_b^T \tag{9a}$$

$$A_b := [v_F^b,\ v_F^b \times a^b,\ v_F^b \times (v_F^b \times a^b)] \tag{9b}$$

$$\hat{A}_n := [\hat{v}^n,\ \hat{v}^n \times \hat{a}^n,\ \hat{v}^n \times (\hat{v}^n \times \hat{a}^n)] \tag{9c}$$

The subsystem Σ_2 represents the translational motion observer, where $K_{pp}, K_{pv}, K_{vp}, K_{vv}, K_{\xi p}$, and $K_{\xi v}$ are observers gains yet to be defined, and $g^n = (0, 0, 9.81)^T$ is the gravity vector in NED.

The system Σ_1–Σ_2 is a feedback interconnection, as illustrated by Fig. 2.

V. Stability Proof

The error dynamics of the attitude observer Σ_1 can be expressed by

$$\dot{\tilde{R}} = RS(\omega^b) - \hat{R}S(\omega_m^b - \hat{b}) - \sigma K_P \hat{J} \tag{10a}$$

$$\dot{\tilde{b}} = -\text{Proj}(\hat{b}, \tau(\hat{J})) \tag{10b}$$

where $\tau(\hat{J}) = -k_I \text{vex}(\mathbb{P}_a(\hat{R}_s^T K_P \hat{J}))$. The equilibrium point $(\tilde{R}, \tilde{b}) = (0, 0)$ was proven to be globally exponentially stable (GES) in [1], with velocities replaced by the magnetic field and assuming that all arguments of $\hat{J}$ were measured values and not estimates.

The error dynamics of the translational motion observer Σ_2 is represented by

$$\dot{\tilde{p}}^n = \tilde{v}^n - K_{pp}\tilde{p}^n - K_{pv}\tilde{v}^n \tag{11a}$$

$$\dot{\tilde{v}}^n = \tilde{a}^n - K_{vp}\tilde{p}^n - K_{vv}\tilde{v}^n \tag{11b}$$

$$\dot{\tilde{a}}^n = -K_{\xi p}\tilde{p}^n - K_{\xi v}\tilde{v}^n + \tilde{d} \tag{11c}$$

where $\tilde{d} = (RS(\omega^b) - \hat{R}S(\omega_m^b - \hat{b}))a^b + (R - \hat{R})\dot{a}^b$. By defining the error variable $\tilde{w} = [(\tilde{p}^n)^T, (\tilde{v}^n)^T, (\tilde{a}^n)^T]^T$, the error dynamics (11) can be written in a more compact form as

$$\dot{\tilde{w}} = (A - KC)\tilde{w} + B\tilde{d} \tag{12}$$

where

$$A = \begin{bmatrix} 0_{6\times3} & I_6 \\ 0_{3\times3} & 0_{3\times6} \end{bmatrix}, \qquad B = \begin{bmatrix} 0_{6\times3} \\ I_3 \end{bmatrix},$$

$$C = \begin{bmatrix} I_6 & 0_{6\times3} \end{bmatrix}, \qquad K = \begin{bmatrix} K_{pp} & K_{pv} \\ K_{vp} & K_{vv} \\ K_{\xi p} & K_{\xi v} \end{bmatrix}.$$

Theorem 1 gives conditions for observer (6)–(7) to be rendered USGES.

Theorem 1: Let σ be chosen to ensure stability according to Lemma 1 in [1] and define $H_K(s) = (Is - A + KC)^{-1}B$. There exists a set $(0, c)$ such that, if K is chosen such that $A - KC$ is Hurwitz and $\|H_K(s)\|_\infty < \gamma$, for $\gamma \in (0, c)$, then the origin of the error dynamics (10)–(12) is USGES as defined by [21] when the initial conditions satisfy $\|\hat{b}(0)\| \leq L_{\hat{b}}$.

Proof: The first part of the proof follows that of Lemma 2 in [1]. However, our expression for $\hat{J}$ is different.

The pair (A, C) is observable and the triple (A, B, C) left-invertible and minimum phase (see Theorem 2 in [4]), so K can always be chosen to satisfy the conditions of the present theorem. It has also been proven that the solutions cannot escape the region $\|\hat{b}\| \leq L_{\hat{b}}$.

The error dynamics (10) can be rewritten as

$$\dot{\tilde{R}} = RS(\omega^b) - \hat{R}S(\omega_m^b - \hat{b}) - \sigma K_P J + \sigma K_P \tilde{J} \tag{13a}$$

$$\dot{\tilde{b}} = -\text{Proj}(\hat{b}, \tau(J)) + \text{Proj}(\hat{b}, \tau(J)) - \text{Proj}(\hat{b}, \tau(\hat{J})) \tag{13b}$$

Consider the Lyapunov function candidate

$$V(\tilde{R}, \tilde{b}) = \frac{1}{2}\|\tilde{R}\|^2 - \ell \text{tr}(S(\tilde{b})R^T\tilde{R}) + \frac{\ell\sigma}{k_I}\|\tilde{b}\|^2$$

which satisfies $\alpha_1(\|\tilde{R}\|^2 + \|\tilde{b}\|^2) \leq V \leq \alpha_2(\|\tilde{R}\|^2 + \|\tilde{b}\|^2)$, where α_1, α_2 are positive constants and $0 < \ell \leq 1$ [1]. Its derivative satisfies

$$\begin{aligned}
\dot{V} \leq & -\alpha_3(\|\tilde{R}\|^2 + \|\tilde{b}\|^2) + \text{tr}(\tilde{R}^T\sigma K_P\tilde{J}) \\
& - \ell\text{tr}(S(\text{Proj}(\hat{b}, \tau(J)) - \text{Proj}(\hat{b}, \tau(\hat{J})))R^T\tilde{R}) \\
& - \ell\text{tr}(S(\tilde{b})R^T\sigma K_P\tilde{J}) \\
& + \frac{2\sigma\ell}{k_I}\tilde{b}^T(\text{Proj}(\hat{b}, \tau(J)) - \text{Proj}(\hat{b}, \tau(\hat{J})))
\end{aligned}$$

We have $\tilde{J} = (A_n - \hat{A}_n)A_b^T = \tilde{A}_n A_b^T$, where

$$\begin{aligned}
\tilde{A_n} = [&v^n - \hat{v}^n, \quad v^n \times a^n - \hat{v}^n \times \hat{a}^n, \\
&v^n \times (v^n \times a^n) - \hat{v}^n \times (\hat{v}^n \times \hat{a}^n)]
\end{aligned}$$

By algebraic manipulation of $\tilde{A_n}$ it can be found that $\|\tilde{A_n}\| \leq h_1\|\tilde{w}\| + h_2\|\tilde{w}\|^2 + h_3\|\tilde{w}\|^3$, where h_1, h_2, h_3 are positive values obtained from the different combinations of $\|a^n\|$ and $\|v^n\|$, which are bounded. It then follows that $\|\sigma K_P\tilde{J}\| \leq s_1(h_1\|\tilde{w}\| + h_2\|\tilde{w}\|^2 + h_3\|\tilde{w}\|^3)$ for some $s_1 > 0$. Still following [1], it is also $\|\text{Proj}(\hat{b}, \tau(J)) - \text{Proj}(\hat{b}, \tau(\hat{J}))\| \leq s_2(h_1\|\tilde{w}\| + h_2\|\tilde{w}\|^2 + h_3\|\tilde{w}\|^3)$ for some $s_2 > 0$.

In virtue of all this, $\dot{V}$ can then be expressed as

$$\begin{aligned}
\dot{V} \leq & -\alpha_3(\|\tilde{R}\|^2 + \|\tilde{b}\|^2) \\
& + \sqrt{3}s_1\|\tilde{R}\|(h_1\|\tilde{w}\| + h_2\|\tilde{w}\|^2 + h_3\|\tilde{w}\|^3) \\
& + \sqrt{6}\ell s_3\|\tilde{R}\|(h_1\|\tilde{w}\| + h_2\|\tilde{w}\|^2 + h_3\|\tilde{w}\|^3) \\
& + \sqrt{6}\ell s_1\|\tilde{b}\|(h_1\|\tilde{w}\| + h_2\|\tilde{w}\|^2 + h_3\|\tilde{w}\|^3) \\
& + \frac{2\sigma\ell s_3}{k_I}\|\tilde{b}\|(h_1\|\tilde{w}\| + h_2\|\tilde{w}\|^2 + h_3\|\tilde{w}\|^3) \\
\leq & -\alpha_3\zeta^2 + h_4\zeta(h_1\|\tilde{w}\| + h_2\|\tilde{w}\|^2 + h_3\|\tilde{w}\|^3)
\end{aligned}$$

for some $h_4 > 0$, where $\zeta := (\|\tilde{R}\|^2 + \|\tilde{b}\|^2)^{1/2}$.

As reported in [22], there is a function $W = \tilde{w}^T P\tilde{w}$, with P positive definite, such that $\dot{W} \leq -\|\tilde{w}\|^2 + \gamma^2\|\tilde{d}\|^2$, where $\tilde{d}$ is defined as in (11) and $\gamma > 0$. $\tilde{d}$ is bounded as $\tilde{d} \leq \sqrt{2}(L_\omega L_a\|\tilde{R}\| + L_a\|\tilde{b}\| + L_{\tilde{b}}L_a\|\tilde{R}\|) + L_{\dot{a}}\|\tilde{R}\|$, where L_ω, L_a, and $L_{\dot{a}}$ are bounds on ω^b, $\|a^b\|$ and $\dot{a}^b$ respectively. Subsequently, $\dot{W} \leq -\|\tilde{w}\|^2 + \gamma^2 q^2\zeta^2$ for some $q > 0$.

Let's now consider function $U = W + \gamma V$ for the whole system. By combining the derivatives of W and V we obtain

$$\begin{aligned}
\dot{U} \leq & -\|\tilde{w}\|^2 + \gamma^2 q^2\zeta^2 \\
& + \gamma(-\alpha_3\zeta^2 + h_4\zeta(h_1\|\tilde{w}\| + h_2\|\tilde{w}\|^2 + h_3\|\tilde{w}\|^3)) \\
= & -\begin{bmatrix}\|\tilde{w}\| & \zeta\end{bmatrix}\begin{bmatrix} q_{11} & q_{12} \\ q_{21} & q_{22}\end{bmatrix}\begin{bmatrix}\|\tilde{w}\| \\ \zeta\end{bmatrix}
\end{aligned}$$

where the matrix components are defined as

$$\begin{aligned}
q_{11} &= 1 \\
q_{12} = q_{21} &= -\frac{1}{2}\gamma h_4(h_1 + h_2\|\tilde{w}\| + h_3\|\tilde{w}\|^2) \\
q_{22} &= -\gamma^2 q^2 + \alpha_3\gamma
\end{aligned}$$

The tunable parameter is γ, so we can say that matrix Q is positive definite if $\gamma < \frac{4\alpha_3}{4q^2 + h_4^2(h_1 + h_2\|\tilde{w}\| + h_3\|\tilde{w}\|^3)^2}$. γ depends on $\|\tilde{w}\|$, so for every different $\|\tilde{w}\|$ it is necessary to choose a different γ to satisfy positive definiteness of Q.

To show USGES of the origin of the system, according to Definition 2.7 in [21], theorem 2 from [23] will be exploited.

Collecting the states in a single vector $x = [\tilde{w}^T, \tilde{R}^T, \tilde{b}^T]^T$ and given the expressions of W and V, it is immediate to see that there exist positive constants $k_1(\gamma), k_2(\gamma)$ such that $k_1(\gamma)\|x\|^2 \leq U \leq k_2(\gamma)\|x\|^2$.

Concerning $\dot{U}$, let us impose positive definiteness by bounding $\|\tilde{w}\|$ instead of γ. The determinant of Q has to be positive, hence the condition

$$h_3\|\tilde{w}\|^2 + h_2\|\tilde{w}\| + h_1 - \sqrt{4\frac{\alpha_3 - \gamma q^2}{h_4^2\gamma}} < 0 \tag{14}$$

$h_1, h_2, h_3, h_4, \alpha_3, q$ have all already been fixed in previous steps, whereas $\gamma > 0$ is still a free parameter. The solution of (14) can be expressed as $\|\tilde{w}\| \leq f(h_1, h_2, h_3, h_4, q, \gamma, \alpha_3) = \Delta$. This corresponds to having $x \in \bar{B}_\Delta$ in theorem 2 from [23]. Since the theorem is valid if Δ can be chosen arbitrarily positive, we have to prove that there always exists a combination of parameters that realises any chosen Δ.

Δ as solution of (14) exists and is positive if $h_1 - \sqrt{4\frac{\alpha_3 - \gamma q^2}{h_4^2\gamma}} < 0$, which is true if $\gamma < \frac{4\alpha_3}{h_1^2 h_4^2 + 4q^2}$. It also has to be imposed that $\gamma \leq \frac{\alpha_3}{q^2}$, so that the square root is real. It's easy to see that $\frac{4\alpha_3}{h_1^2 h_4^2 + 4q^2} < \frac{\alpha_3}{q^2}$ is always true, so only $\gamma < \frac{4\alpha_3}{h_1^2 h_4^2 + 4q^2}$ is necessary. This means that, for any $\gamma \in (0, \frac{4\alpha_3}{h_1^2 h_4^2 + 4q^2})$, the parabola represented by (14) will cross the horizontal axis at any positive value. In other words, for any chosen $\Delta > 0$, there is a γ such that the solution of (14) is $\|\tilde{w}\| \leq \Delta$.

At this point $\dot{U}$ is negative definite in function of γ, which in turn depends on Δ, so it can be expressed as

$\dot{U} \leq -k_3(\Delta)\|x\|^2$, where $k_3(\Delta) > 0$ is a constant that depends on the chosen Δ.

It can also be verified that

$$\lim_{\Delta\to\infty} \frac{k_1(\gamma(\Delta))\Delta^2}{k_2(\gamma(\Delta))} = \infty \tag{15}$$

Both k_1 and k_2 depend on the function U, which is explicitly linear in γ. However, U is also function of P, that depends on γ. Given that $\gamma \to 0$ as $\Delta \to \infty$ and the eigenvalues of P have the same rate of convergence to zero [22], [24], both k_1 and k_2 are functions of γ of the same order for the scope of (15), which is thus verified.

All hypotheses of theorem 2 from [23] are satisfied, so it can be concluded that the origin of the error dynamics (10)–(12) is USGES. ■

VI. Case Study

The dynamics of a UAV is here simulated, together with the information available from the sensors, and the observer (6)–(8) is verified based on these data. It is assumed that machine vision can provide the required v_F^b. The matrix $\hat{J}$ is first calculated based on information coming from magnetometers and accelerometers: the magnetic field vector m^n is assumed constant, with a value corresponding to Earth's magnetic field in Trondheim, Norway. At time $t = 90$s a drift in the magnetometers' readings is simulated, and at $t = 100$s they are replaced by machine vision, so v_F^b and $\hat{v}^n$ take the place of m^b and m^n. In this way the system is shown to be fault-tolerant. Zero-mean Gaussian white noise is added to all measurements, which are assumed to be available at the same rate of 100 Hz. The GPS measurement error $\nu[n]$ is modeled as a Gauss-Markov process by $\nu[n+1] = e^{-k_{\text{GPS}}T_s}\nu[n] + \eta_{\text{GPS}}[n]$, where η_{GPS} is zero-mean Gaussian white noise, $1/K_{\text{GPS}}$ is the time constant of the process, and T_s is the sampling time. Table I reports the values for such parameters.

TABLE I
GAUSS-MARKOV ERROR MODEL PARAMETERS FOR GPS MEASUREMENTS

Direction	*Std. Dev.* η_{GPS} (m)	$1/k_{\text{GPS}}$ (s)	T_s (s)
North	0.21	1100	1.0
East	0.21	1100	1.0
Altitude	0.40	1100	1.0

The gyro bias is limited by $\|b\| < L_b = 2°$/s, and $L_{\hat{b}} = 2.1°$/s is used for the projection. The observer gains are initialised with $K_P = \text{diag}(10, 10, 10)$, $\sigma = 1$, $k_I = 0.02$, $K_{pp} = 100I_3$, $K_{pv} = I_3$, $K_{vp} = 0.1I_3$, $K_{vv} = 8I_3$, $K_{\xi p} = I_3$, and $K_{\xi v} = 5I_3$. At time $t = 100$s some of the gains are changed: $K_P = \text{diag}(1, 1, 1)$, $K_{vv} = 10I_3$, and $K_{\xi p} = 0.1I_3$.

The simulation results are illustrated in Figs. 3–7.

VII. Conclusions and Future Work

A fault-tolerant nonlinear observer for estimating attitude, position, velocity, acceleration and gyro bias of a UAV was proposed and successfully verified with simulations, after having proven that its origin is USGES. In future developments Assumption 4 will be dropped and it will be tried to prove stability of the observer even when the roll and pitch angles are extracted from the estimated rotation matrix. Machine vision will also be implemented and full-scale experiments with UAVs will be performed, so that the observer can be verified on real data.

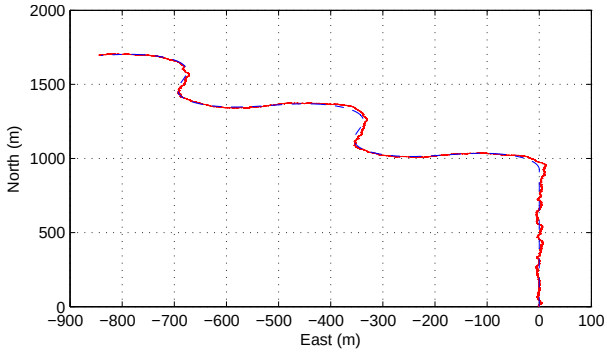

Fig. 3. True (blue, dashed) and estimated (red, solid) North and East coordinates

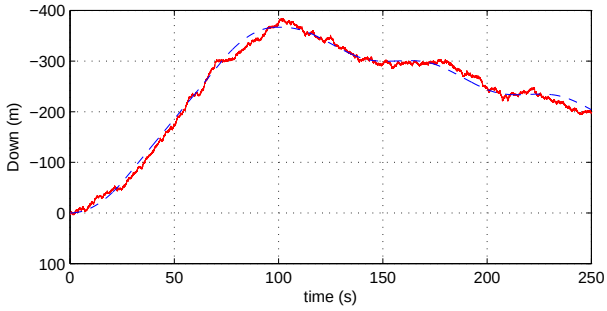

Fig. 4. True (blue, dashed) and estimated (red, solid) Down coordinate

Acknowledgements

This work was partially supported by the Norwegian Research Council through the Centre for Autonomous Marine Operations and Systems (AMOS) at the Norwegian University of Science and Technology.

References

[1] H. Grip, T. Fossen, T. Johansen, and A. Saberi, "A nonlinear observer for integration of GNSS and IMU measurements with gyro bias estimation," *American Control Conference (ACC)*, pp. 4607–4612, 2012.

[2] P. Batista, C. Silvestre, and P. Oliveira, "GES attitude observers - Part I: Multiple general vector observations," *Proceedings of the 18th IFAC World Congress*, vol. 18, pp. 2985–2990, 2011.

[3] ——, "GES attitude observers - Part II: Single vector observations," *Proceedings of the 18th IFAC World Congress*, vol. 18, pp. 2991–2996, 2011.

[4] H. Grip, T. Fossen, T. Johansen, and A. Saberi, "Attitude estimation using biased gyro and vector measurements with time-varying reference vectors," *IEEE Transactions on Automatic Control*, vol. 57, no. 5, pp. 1332–1338, 2012.

[5] R. Mahony, T. Hamel, and J. Pflimlin, "Nonlinear complementary filters on the special orthogonal group," *IEEE Transactions on Automatic Control*, vol. 53, no. 5, pp. 1203–1218, 2008.

[6] R. Mahony, T. Hamel, J. Trumpf, and C. Lageman, "Nonlinear attitude observers on SO(3) for complementary and compatible measurements: A theoretical study," *Proceedings of the 48th IEEE Conference on Decision and Control*, pp. 6407–6412, 2009.

[7] S. Salcudean, "A globally convergent angular velocity observer for rigid body motion," *IEEE Transactions on Automatic Control*, vol. 36, no. 12, pp. 1493–1497, 1991.

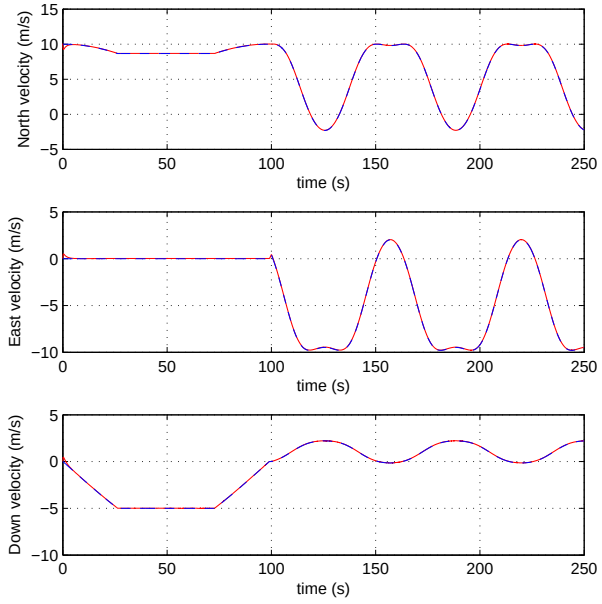

Fig. 5. True (blue, dashed) and estimated (red, solid) velocity in NED coordinates

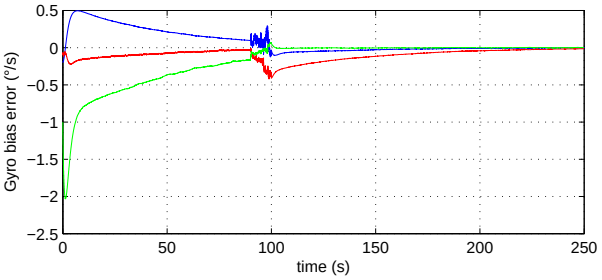

Fig. 6. Error between estimated and true gyro bias. At time $t = 100$s the magnetometers fail and are replaced by camera measurements

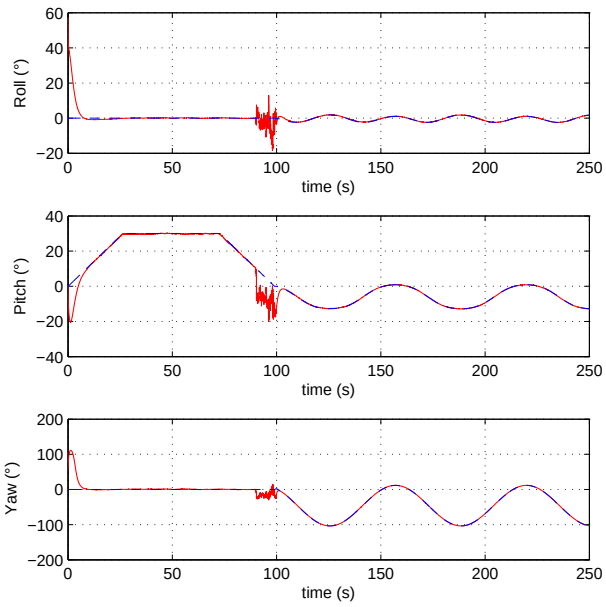

Fig. 7. True (blue, dashed) and estimated (red, solid) Euler angles. At time $t = 100$s the magnetometers fail and are replaced by camera measurements

objects," *IEEE Transactions on Systems, Man, and Cybernetics, Part C: Applications and Reviews*, vol. 42, no. 6, pp. 1752 – 1762, 2012.

[8] J. Thienel and R. Sanner, "A coupled nonlinear spacecraft attitude controller and observer with an unknown constant gyro bias and gyro noise," *IEEE Transactions on Automatic Control*, vol. 48, no. 11, pp. 2011–2015, 2003.

[9] M. Hua, "Attitude estimation for accelerated vehicles using GPS/INS measurements," *Control Engineering Practice*, vol. 18, no. 7, pp. 723–732, 2010.

[10] H. Grip, T. Fossen, T. Johansen, and A. Saberi, "Nonlinear observer for GNSS-aided inertial navigation with quaternion-based attitude estimation," *American Control Conference (ACC)*, pp. 272–279, 2013.

[11] S. Soatto, R. Frezza, and P. Perona, "Motion estimation via dynamic vision," *IEEE Transactions on Automatic Control*, vol. 41, no. 3, pp. 393–414, 1996.

[12] S. Soatto and P. Perona, "Recursive 3-d visual motion estimation using subspace constraints," *International Journal of Computer Vision*, vol. 22, no. 3, pp. 235–259, 1997.

[13] P. Gurfil and H. Rotstein, "Partial aircraft state estimation from visual motion using the subspace constraints approach," *Journal of Guidance, Control, and Dynamics*, vol. 24, no. 5, pp. 1016–1028, 2001.

[14] D. Diel, P. DeBitetto, and S. Teller, "Epipolar constraints for vision-aided inertial navigation," *IEEE Workshop on Application of Computer Vision*, pp. 221–228, 2005.

[15] J. Kehoe, A. Watkins, R. Causey, and R. Lind, "State estimation using optical flow from parallax-weighted feature tracking," *AIAA Guidance, Navigation, and Control Conference*, 2006.

[16] S. Zingg, D. Scaramuzza, S. Weiss, and R. Siegwart, "Mav navigation through indoor corridors using optical flow," *IEEE International Conference on Robotics and Automation (ICRA)*, pp. 3361–3368, 2010.

[17] M. Mammarella, G. Campa, M. Fravolini, and M. Napolitano, "Comparing optical flow algorithms using 6-dof motion of real-world rigid

[18] M. Sonka, V. Hlavac, and R. Boyle, *Image processing, analysis, and machine vision*. Stamford, CT: Cengage Learning, 2008.

[19] M. Krstic, I. Kanellakopoulos, and P. Kokotovic, *Nonlinear and Adaptive Control Design*. New York: Wiley, 1995.

[20] M. Shuster and S. Oh, "Three-axis attitude determination from vector observations," *Journal of Guidance, Control and Dynamics*, vol. 4, no. 1, pp. 70–77, 1981.

[21] A. Loria and E. Panteley, "Cascaded nonlinear time-varying systems: analysis and design," in *Advanced Topics in Control Systems Theory*. London: Springer-Verlag (F. Lamnabhi-Lagarrigue, A. Loria and E. Panteley Eds.), 2004, ch. 2, pp. 23–64.

[22] H. Grip, A. Saberi, and T. Johansen, "Observers for interconnected nonlinear and linear systems," *Automatica*, vol. 48, no. 7, pp. 1339–1346, 2012.

[23] E. Grotli, A. Chaillet, and J. Gravdahl, "Output control of spacecraft in leader follower formation," *Proceedings of the 47th IEEE Conference in Decision and Control*, pp. 1030–1035, 2008.

[24] W. Kwon, Y. Moon, and S. Chul, "Bounds in algebraic riccati and lyapunov equations: a survey and some new results," *International Journal of Control*, vol. 64, no. 3, pp. 377–389, 1996.

APPENDIX

The parameter projection $\text{Proj}(\cdot,\cdot)$ is defined as:

$$\text{Proj}(\hat{b},\tau) = \begin{cases} \left(I - \frac{c(\hat{b})}{\|\hat{b}\|^2}\hat{b}\hat{b}^T\right)\tau, & \|\hat{b}\| \geq L_b,\ \hat{b}^T\tau > 0 \\ \tau, & \text{otherwise} \end{cases}$$

where $c(\hat{b}) = \min\{1, (\|\hat{b}\|^2 - L_b^2)/(L_{\hat{b}}^2 - L_b^2)\}$. This operator is a special case of that from Appendix E of [19]. Some of its properties, used in this paper, are reported here: (i) $\text{Proj}(\cdot,\cdot)$ is locally Lipschitz continuous, (ii) $\|\hat{b}\| \geq L_{\hat{b}} \Rightarrow \hat{b}^T\text{Proj}(\hat{b},\tau) \leq 0$, (iii) $\|\text{Proj}(\hat{b},\tau)\| \leq \|\tau\|$, and (iv) $-\tilde{b}^T\text{Proj}(\hat{b},\tau) \leq -\tilde{b}^T\tau$.